Analyst

Cite this: *Analyst*, 2012, **137**, 4171

www.rsc.org/analyst

PAPER

Ultrasensitive aptamer biosensor for arsenic(III) detection in aqueous solution based on surfactant-induced aggregation of gold nanoparticles†

Yuangen Wu,‡[ab] Le Liu,‡[a] Shenshan Zhan,[a] Faze Wang[a] and Pei Zhou*[a]

Received 29th May 2012, Accepted 13th July 2012
DOI: 10.1039/c2an35711a

This paper reports the colorimetric and resonance scattering (RS)-based biosensor for the ultrasensitive detection of As(III) in aqueous solution *via* aggregating gold nanoparticles (AuNPs) by the special interactions between arsenic-binding aptamer, target and cationic surfactant. Aptamers and the cationic surfactant could assemble to form a supramolecule, which prevented AuNPs from aggregating due to the exhaustion of cationic surfactant. The introduction of As(III) specifically interacted with the arsenic-binding aptamer to form the aptamer–As(III) complex, so that the following cationic surfactant could aggregate AuNPs and cause the remarkable change in color and RS intensity. The results of circular dichroism (CD) and scanning probe microscope (SPM) testified to the formation of the supramolecule and aptamer–As(III) complex, and the observation of transmission electron microscope (TEM) further confirmed that the aggregation of AuNPs could be controlled by the interactions among the aptamer, As(III) and cationic surfactant. The variations of absorbance and RS intensity were exponentially related to the concentration of As(III) in the range from 1 to 1500 ppb, with the detection limit of 40 ppb for the naked eye, 0.6 ppb for colorimetric assay and 0.77 ppb for RS assay. Additionally, the speed of the present biosensor was rapid, and it also exhibited high selectivity over other metal ions with an excellent recovery for detection in real water samples, suggesting that the proposed biosensor will play an important role in environmental detection.

1. Introduction

Arsenic is a naturally occurring element with wide distribution in both organic and inorganic forms. Exposure to arsenic can cause a number of diseases such as skin damage or problems with circulatory systems, and a high risk of getting cancer.[1] Inorganic arsenic is considered to be the most toxic form of the element, and it is found in groundwater and surface water as well as in many foods.[2] Recent studies have shown that arsenic poisoning may be worse than previously thought, with as many as 77 million people possibly exposed to arsenic-contaminated water in Bangladesh alone.[3] Although arsenic exists in many different chemical forms in nature, they are found almost exclusively as arsenite (As(III) as H_3AsO_3) and arsenate (As(V) as H_3AsO_4) in water.[4] It is more significant and attractive to detect As(III) than As(V) in water due to the higher toxicity and stability of As(III). The World Health Organization's arsenic guideline value for drinking water is 10 ppb. Recent reviews have summarized some detection methods for such levels of arsenic.[5,6] The most popular methods for arsenic detection require sophisticated equipment and a long analysis time, so they are neither readily available in developing countries nor capable of on-site field detection. To address these problems, some novel chemosensors and biosensors have been developed.[7,8] For example, Ray and co-workers developed a highly sensitive sensor for arsenic detection with a detection limit of 3 ppt using a dynamic light scattering assay.[9] Others used genetically modified *Escherichia coli* cells and presented a pH-based biosensor for the detection of arsenic in drinking water.[10] However, these methods usually needed some reactions or modification, thus some of them may be susceptible to the surrounding conditions. Therefore, it is highly necessary to develop simple and stable methods to detect trace arsenic in the environment.

Functional nucleic acids, including oligonucleotide ligands, aptamers and riboswitches, have been widely used as the target recognition elements in sensing applications due to their competitive advantages over other biological tools such as antibodies, enzymes, peptides, carbohydrates *etc.*[11,12] Aptamers are the *in vitro*-selected artificial single-strand RNA or DNA oligonucleotides with unique conformations that can distinctly bind to a broad range of targets.[13] Combined with some signal transductions (*e.g.* colorimetric, fluorescent and electrochemical

[a]*Key Laboratory of Urban Agriculture (South), Ministry of Agriculture, and School of Agriculture and Biology, and School of Environmental Science and Engineering, and Bor S. Luh Food Safety Research Center, Shanghai Jiao Tong University, Shanghai, 200240, China. E-mail: zhoupei@sjtu.edu.cn; Fax: +86-21-34205762; Tel: +86-21-34205762*
[b]*School of Chemistry and Chemical Engineering, Guizhou University, Guiyang, 550025, Guizhou, China. Fax: +86-851-4732925; Tel: +86-851-4732861*

† Electronic supplementary information (ESI) available: Supplementary figures. See DOI: 10.1039/c2an35711a

‡ These authors contributed equally to this work.

signals), various aptamer-based biosensors have been developed to detect a large number of analytes such as metal ions, organic dyes, amino acids, nucleotides, proteins, or even cells and bacteria.[14–16] In particular, aptamers have been regarded as promising tools in environmental monitoring due to the real-time and on-site detection of heavy metals including lead, mercury, silver and uranium.[17–19] Recently, Kim and co-workers have *in vitro* selected the arsenic-binding DNA aptamer (named Ars-3 aptamer)[20] using an affinity column based on the systematic evolution of ligands by exponential enrichment (SELEX) process. Such a single-strand DNA aptamer contains 100 nucleotides and possesses the highest affinity to As(III) with a dissociation constant (K_d) of 7.05 nM. Owing to the long chain of the Ars-3 aptamer, it is hard to modify them with fluorescent agents or other reported molecules for signal transduction. Up to now, reports involving aptamer-based biosensors for arsenic detection have been rare. Therefore, it is attractive and a challenge to develop new signal transduction for long-chain aptamers in the design of biosensors.

Gold nanoparticles (AuNPs) are the ideal materials for signal transduction with some superior characteristics, and they have attracted particular interest in the design of biosensors.[21–25] The popular signals of AuNPs are colorimetric and resonance scattering (RS) assays based on their transformation from disperse to aggregated.[26–30] The aggregation of AuNPs will increase the size of particles in solutions, which causes the remarkable change in absorbance and RS intensity. Base on this principle, some simple and rapid sensors have been developed to detect a variety of targets.[31,32] To aggregate AuNPs, the relevant nanoparticles are usually modified with functional DNAs, and they will aggregate *via* the hybridization induced by the special interactions between the functional DNAs and targets. Another common approach utilizes unmodified nanoparticles that are aggregated by the high concentration of salts (*e.g.* sodium). These two approaches, however, may suffer from being time-consuming and having relatively poor detection limits.[33] Recently, some reports demonstrated that water-soluble cationic polymers could control the assembly of AuNPs.[34] These evidences have enabled us to develop a novel, efficient aptamer biosensor for the colorimetric analysis of As(III) with a detection limit of 5.3 ppb.[35]

In this paper, a more sensitive and selective aptamer biosensor was presented to detect As(III) in aqueous solution. Hexadecyltrimethylammonium bromide (CTAB), a cationic surfactant, was considered as an efficient material to aggregate the AuNPs. Recent researches have demonstrated that CTAB can be used to prepare AuNPs with controllable sizes and shapes.[36–38] CTAB displays two useful features in the present biosensor: one of the useful properties of CTAB lies in its positive charge, which can be employed to aggregate AuNPs, and another is that it can assemble DNAs to form some supramolecule with certain nanostructures.[39–41] For example, some studies have shown that long-chain, single-stranded DNA formed cubic nanostructures with CTAB, whereas long-chain, double-stranded DNA formed hexagonal nanostructures.[42] These useful properties endow CTAB with special functions in the present biosensor: it not only aggregates the AuNPs, but also controls their aggregation *via* its competitive binding to aptamers. Scheme 1 shows the concept and process of the biosensor for arsenic detection. In the absence of As(III), the Ars-3 aptamers are free and can assemble with CTAB to form some supramolecule, and thus the subsequent AuNPs cannot aggregate due to the lack of CTAB. On adding As(III), the Ars-3 aptamers are exhausted firstly due to the formation of an aptamer–As(III) complex, so that the following CTAB can aggregate AuNPs, which leads to the remarkable signal change in absorbance and RS intensity. The signal variation of solution depends on the concentration of CTAB, which is in turn conditioned directly by the content of As(III). Therefore, this strategy makes it possible to detect As(III) by colorimetric and RS assays. It is expected that our method can be extended to detect other metal ions, proteins and small molecules.

2. Experimental

2.1. Chemicals and materials

The sequence of Ars-3 aptamer is referenced in the previous literatures,[20] and was synthesized by Sangon Biotechnology Co., Ltd. (Shanghai, China). Its sequence is 5′-GGTAATACG ACTCACTATAGGGAGATACCAGCTTATTCAATTTTAC AGAACAACCAACGTCGCTCCGGGTACTTCTTCATCGA GATAGTAAGTGCAATCT-3′. Before use, the Ars-3 aptamer was dissolved in 50 mM *N*-(2-hydroxyethyl) piperazine-*N*-2-ethanesulfonic acid (HEPES) buffer solution of pH 7.2. Hexadecyltrimethylammonium bromide (CTAB), trimethyl(tetradecyl)ammonium bromide (TTAB), hexadecylpyridinium chloride monohydrate (HPCM) and tridodecylmethylammonium chloride (TDAC) were obtained from Sigma-Aldrich (Milwaukee, WI, USA). $HAuCl_4$ and 3-(*N*-morpholino) propanesulfonic acid (MOPS) were obtained from Sangon Biotechnology Inc. (Shanghai, China). The 96-well microplate was purchased from Thermo Fisher Scientific Inc. (Nunclon, Denmark). Unless otherwise mentioned, all other reagents were of analytical grade and used without further purification or treatment. Ultrapure water (Milli-Q plus, Millipore Inc., Bedford, MA) was used throughout.

2.2. Instrumentation

A model F-4500 fluorescence spectrophotometer (Hitachi, Japan) was used to record the RS intensity, with the excitation slit of 5 nm and an emission slit of 2.5 nm, and a PMT voltage of 700 V. Colorimetric assays were recorded on a Microplate

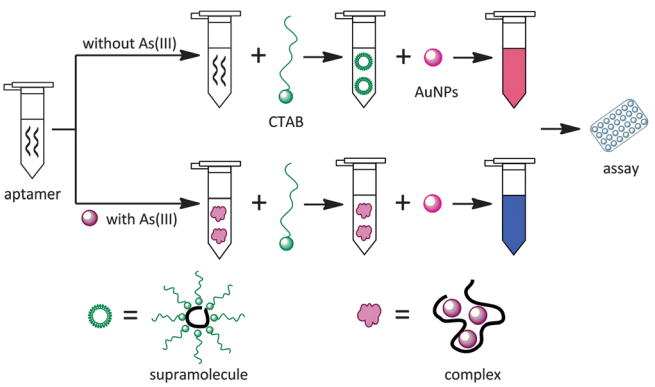

Scheme 1 Illustration of the biosensor for As(III) detection based on the surfactant-induced aggregation of AuNPs.

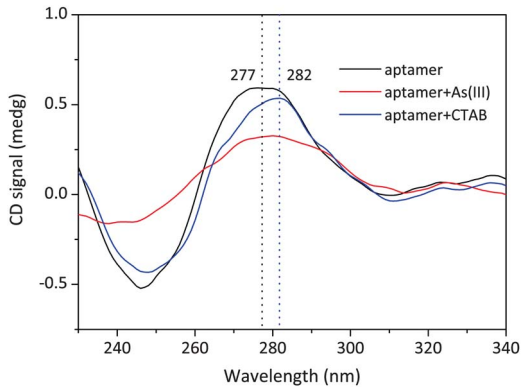

Fig. 1 CD spectra of Ars-3 aptamer solutions treated with CTAB and As(III). Experimental conditions: 500 nM Ars-3 aptamer, 50 μM CTAB and 2000 ppb As(III).

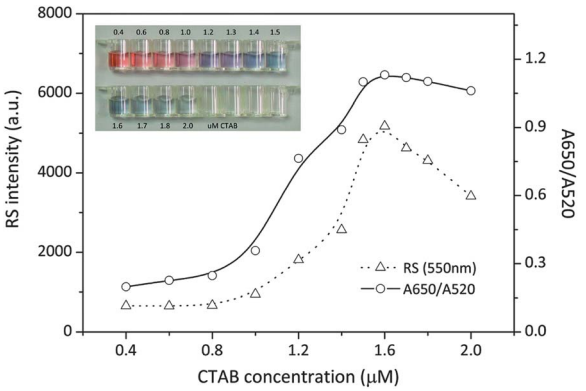

Fig. 3 Effect of CTAB concentrations on the aggregation of AuNPs. Inset: visual colour changes of AuNPs solutions treated with increasing concentrations of CTAB.

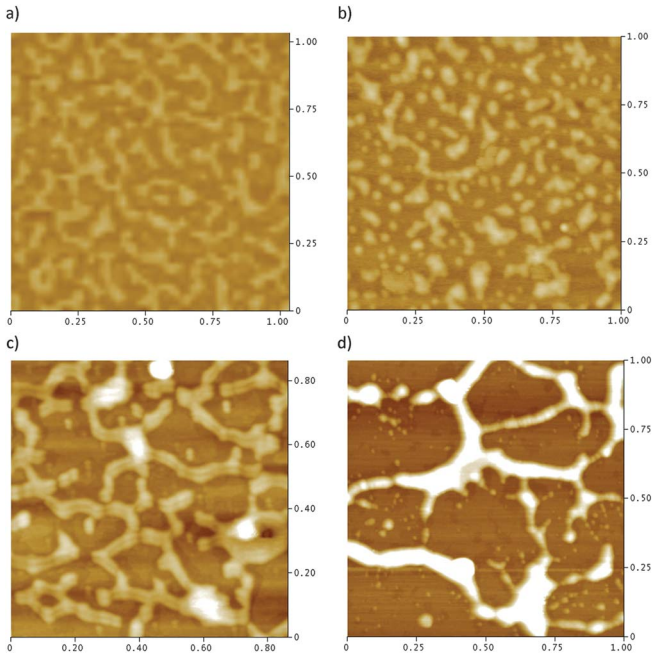

Fig. 2 Scanning probe microscope (SPM) observation of the solutions containing: (a) 500 nM Ars-3 aptamer; (b) 500 nM Ars-3 aptamer + 1000 ppb As(III); (c) 500 nM Ars-3 aptamer + 50 μM CTAB; and (d) 500 nM Ars-3 aptamer + 50 μM CTAB + 1000 ppb As(III).

Spectro-photometer M200 Pro (Tecan Group Ltd, Switzerland). Circular dichroism (CD) spectra were collected with the J-815 Circular Dichroism Spectropolarimeter (Jasco, Japan) in HEPES buffer (50 mM, pH 7.2) to characterize the structure change of aptamers at room temperature. The optical chamber (0.5 mL volume) was utilized. The scanning speed was 100 nm min^{-1}. The CD spectra were collected in the range of 200–400 nm. A Multimode Nanoscope IIIa scanning probe microscope (SPM) (Digital Instrument Inc., NY, USA) was used to observe the images of the nanoparticles, and the procedure for samples pre-treatment is referenced in our previous report.[43] An analytical transmission electron microscope (TEM) JEM-2010HT (Hitachi, Japan) was used to observe the images of AuNPs. The average size of the nanoparticles was determined by photon correlation spectroscopy (PCS) (Malvern Instruments, UK).

2.3. Preparation of AuNPs

AuNPs with different sizes were synthesized by controlling the ratio of sodium citrate and $HAuCl_4$ following some recent reports.[44–46] All glassware used in this procedure was cleaned in a bath of freshly prepared 3 : 1(v/v) HNO_3–HCl, then rinsed thoroughly in ultrapure water and dried in air. AuNPs were prepared by adding 0.5–6.0 mL of 1% (w/v) trisodium citrate to a boiling solution of $HAuCl_4$ (100 mL, 0.01% (w/w)) and stirred for 30 min, where, within the time, the color of the solution changed from light grey, blue, purple, to wine red. The mixture continued to stir for 10 min after removal from the heater. Finally, the cooled solution was filtered using a 0.2 μm ultrafiltration membrane to remove aggregated particles, and then stored in dark glass bottles at 4 °C for further use.

2.4. Procedure for As(III) determination

An appropriate volume of 500 nM Ars-3 aptamer solution and 5 μL $NaAsO_2$ solution [As(III)] with varying concentrations were mixed thoroughly in a 2 mL plastic tube, and then diluted to 390 μL with MOPS buffer (pH 7.0) and incubated at 25 °C for 30 min. To the blank sample was added 5 μL of ultrapure water instead of As(III) solution. Subsequently, 10 μL CTAB was added into the above mixed solutions and incubated at 25 °C for another 30 min. Finally, 100 μL AuNPs stock solution was added to give a final volume of 500 μL. After incubation at 25 °C for 5 min, 200 μL of the above samples were moved into a 96-well microplate for colorimetric assay. The absorption spectra (the wavelength range from 400 to 800 nm) and absorbance values at 520 nm (A_{520}) and 650 nm (A_{650}) were measured by Microplate Spectro-photometer M200 Pro. The ratio of A_{650}/A_{520} in sample solutions (A) and the blank solution without arsenic (A_0) were recorded to indicate the aggregation of AuNPs. The value of $\Delta A = A - A_0$ was calculated to evaluate As(III) detection throughout. For the RS assay, the intensity was recorded by means of synchronous scanning of the excitation wavelength λ_{ex} and emission wavelength λ_{em} ($\lambda_{ex} - \lambda_{em} = \Delta\lambda = 0$) on the fluorescence spectrophotometer. The RS intensity at 550 nm in

Table 1 The efficiency of AuNPs aggregation using different cationic surfactants and salt

Cationic surfactants	AuNPs change to purple[a]	AuNPs change to blue	Reaction time/min
CTAB	1.1 μM	1.6 μM	<5
HPCM	0.6 μM	1.0 μM	<5
TDAC	1.0 μM	1.6 μM	5–10
TTAB	2.4 μM	3.2 μM	5–10
Others (NaCl)	50 mM	70 mM	>10

[a] The quantity of AuNPs for aggregation was about 30 nmol.

sample solutions (I) and the blank solution without arsenic (I_0) were recorded. The value of $\Delta I = [I - I_0]/I_0$ was calculated. To test the selectivity of the biosensor, other metal salts including Na_2HAsO_4 [As(v)], $Pb(NO_3)_2$, $Hg(NO_3)_2$, $Cd(NO_3)_2$, $AgNO_3$, $CaCl_2$, $ZnCl_2$, $MgSO_4$, $MnSO_4$, $NiSO_4$, $CuSO_4$ and $FeSO_4$ were used.

3. Results and discussion

3.1. Interactions among aptamer, CTAB and arsenic(III)

According to the principle of the present biosensor, the Ars-3 aptamer would interact with the target (*e.g.* As(III)) and CTAB to form the aptamer–As(III) complex and supramolecule, respectively. To confirm the interactions among aptamer, CTAB and As(III), CD measurements were utilized to monitor the confirmation change of the aptamer in the solutions. Fig. 1 shows the CD spectra of aptamer solutions treated with CTAB and As(III). The Ars-3 aptamer (generally B-DNA) has a negative peak at 240–260 nm and a positive peak at 270–290 nm, which is in accordance with previous reports.[35] After the addition of As(III), the value of negative and positive peaks were decreased, but the location of the peaks did not change. This result indicated that As(III) could bind to the Ars-3 aptamer, which interfered with bases from the transition of strong $\pi \rightarrow \pi^*$ with ribodesose, thus resulting in the decrease of the CD peak. In the presence of CTAB, the peak area of the CD spectrum did not change, but an obvious bathochromic shift (~5 nm) in the positive peak was observed. The bathochromic shift indicated that an electron transfer occurred from CTAB to the lowest unoccupied molecular orbital of the bases in the aptamer. Such a characteristic feature was evidence for the interaction of CTAB with the DNA bases.

Table 2 Average size of AuNPs in sensing solutions treated with different concentrations of As(III)[a]

Order	Sample	Average size/nm	RSD (%)
1	AuNPs	18.23	0.46
2	AuNPs + CTAB	473.6	1.65
3	AuNPs + aptamer + CTAB	21.34	1.26
4	Sample 3 + 1 ppb As(III)	23.79	0.97
5	Sample 3 + 10 ppb As(III)	32.44	2.23
6	Sample 3 + 50 ppb As(III)	56.74	1.54
7	Sample 3 + 100 ppb As(III)	83.46	1.77
8	Sample 3 + 200 ppb As(III)	98.30	0.18
9	Sample 3 + 500 ppb As(III)	152.4	0.19
10	Sample 3 + 1000 ppb As(III)	222.7	0.76

[a] Experimental conditions: 10 nM Ars-3 aptamer and 1.1 μM CTAB.

To further confirm the formation of the aptamer–As(III) complex and supramolecule, the Ars-3 aptamer solutions treated

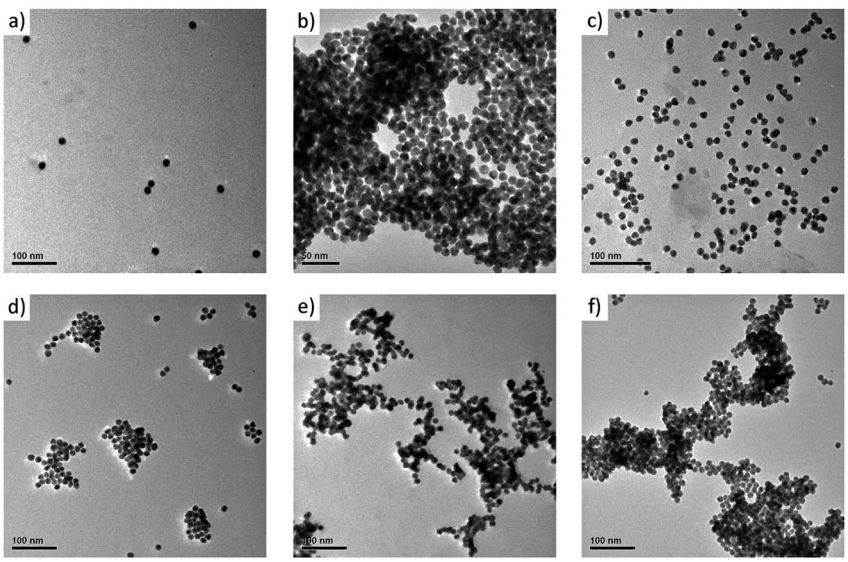

Fig. 4 Transmission electron microscope (TEM) images of the AuNPs solutions treated with different substances: (a) blank AuNPs; (b) AuNPs + 1.1 μM CTAB; (c) AuNPs + 10 nM Ars-3 aptamer + 1.1 μM CTAB; (d) sample c + 100 ppb As(III); (e) sample c + 500 ppb As(III); (f) sample c + 1000 ppb As(III).

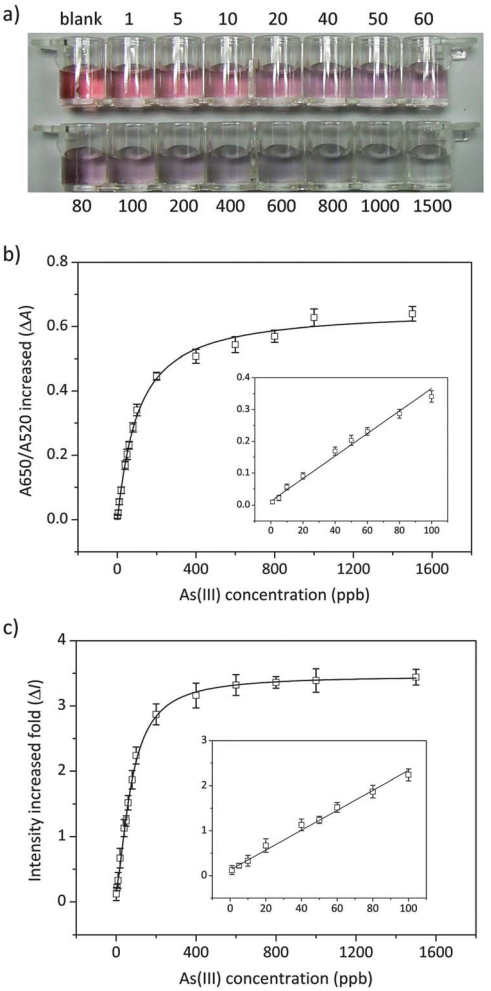

Fig. 5 Sensitivity of the biosensor for As(III) detection using CTAB to aggregate AuNPs: (a) visual colour changes of the sensing solutions treated with 0, 1, 5, 10, 20, 40, 50, 60, 80, 100, 200, 400, 600, 800, 1000 and 1500 ppb As(III); calibration curves of the biosensor based on colorimetric (b) and RS (c) assays. The curves were fitted to a Hill plot with a correlation coefficient of 0.997 (b) and 0.998 (c). Inset: the values of ΔA and ΔI at low As(III) concentrations, which were fitted to a linear plot with a correlation coefficient of 0.989 (b) and 0.994 (c).

Table 3 Sensitivity of the biosensor for the colorimetric detection of As(III) under different size of AuNPs and cationic surfactants

Cationic surfactants	AuNPs size/nm	LOD/ppb	Linear range/ppb
CTAB	18	0.6	1–100
CTAB	30	4.1	1–200
CTAB	50	5.5	10–60
CTAB	80	14.1	1–200
HPCM	18	1.2	5–200
TDAC	18	2.6	10–200
TTAB	18	2.3	5–100
Others (NaCl)	18	7.1	10–400

with CTAB and As(III) were characterized by SPM (Fig. 2). The shape of the Ars-3 aptamer was a linear chain and it was distributed evenly in the solutions. On adding As(III) into the aptamer solution, the shape of the DNAs had changed to some extent. Some aptamers interacted with As(III) to form irregular nanoparticles, which was evidence for the formation of the aptamer–As(III) complex. In the presence of CTAB, however, the shape of the aptamer changed greatly. Some reticular macromolecules with a branched shape could be observed in the solution, which demonstrated the formation of the supramolecule by the aptamer and CTAB. The forces for maintaining such a supramolecule might be ascribed to the electrostatic force between the positive hydrophilic head of CTAB and the negative phosphate backbone of DNAs. In addition, the effect of As(III) on the supramolecule was also investigated. As shown in Fig. 2d, the shape of the supramolecule became dense and its diameter had increased. This evidence showed that As(III) can strengthen the interaction between the aptamer and CTAB.

3.2. Aggregation AuNPs by aptamer, CTAB and arsenic(III)

Electrosteric stabilization is the major factor for AuNPs to remain dispersed in aqueous solution. Generally, the positively charged material, such as cationic polymer and high concentration of sodium, can disturb the charge balance of the AuNPs and cause them aggregate. Herein, CTAB was employed to aggregate AuNPs. The aggregation principle for CTAB may be similar to that of cationic polymers. To investigate the efficiency of aggregation, varying concentrations of CTAB from 0.4 to 2.0 μM were added into AuNPs solutions, and the RS intensity and A_{650}/A_{520} were recorded. As shown in Fig. 3, the color of the AuNPs solutions changed gradually from wine red, purple, to blue. The values of RS intensity and A_{650}/A_{520} increased until the concentration of CTAB reached 1.6 μM. At this point, all AuNPs aggregated thoroughly. With further increase in the CTAB concentration, the values decreased significantly. The reason for this phenomenon was that the AuNPs aggregated thoroughly to form large particles at a high concentration of CTAB, and most of them would precipitate in solutions.

Different cationic surfactants and salt were also considered to aggregate AuNPs. As shown in Table 1, all of selected cationic surfactants could aggregate AuNPs, but their efficiencies were clearly different. These variations may be attributed to the different chemical structures of the cationic surfactants; in particular, the length of the alkyl chains may affect the interaction between the AuNPs and cationic surfactants. CTAB and HPCM contain 16 carbons in their alkyl chains, and they displayed the highest efficiency in the aggregation of AuNPs. The difference between them lies in their positively charged groups, where the one in the pyridinium group of HPCM seemed to have a higher efficiency than that of CTAB. When the alkyl chain decreased to 14 carbons (TTAB in Table 1), the efficiency of the AuNPs aggregation also declined obviously. Interestingly, the multiple alkyl chain would be beneficial to aggregate AuNPs. For example, TDAC has three alkyl chains with 12 carbons and also exhibited a relatively high efficiency. In the case of salt, however, the efficiency of AuNPs aggregation was far less than that of the cationic surfactants, based on the evaluation of the minimum concentrations and reaction times for AuNPs aggregation. Therefore, CTAB and HPCM can be used as efficient materials to aggregate AuNPs, and CTAB will be the preferred cationic surfactant because of its low price and safety.

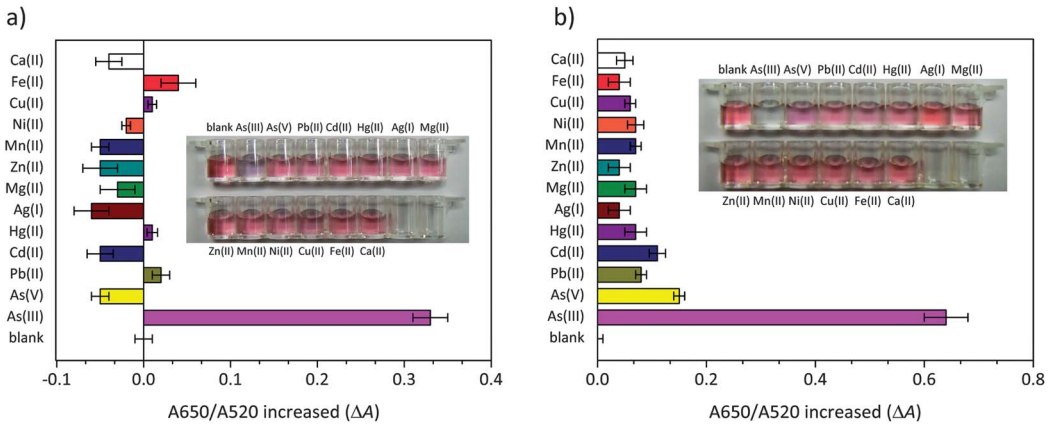

Fig. 6 Selectivity of the biosensor for As(III) detection using CTAB to aggregate AuNPs. The concentrations of metal ions were 100 ppb (a) and 1000 ppb (b). Inset: visual colour changes of the sensing solutions treated with various metal ions.

To confirm the supposed principle of the present biosensor, TEM was employed to characterize the aggregation of AuNPs. Fig. 4 displays the images of AuNPs solutions treated with different substances, and the results testified that the aggregation of AuNPs was controlled by the interactions between the aptamer, CTAB and As(III). Free AuNPs dispersed evenly with an average particle diameter of 15 nm (a). The introduction of CTAB could cause the complete aggregation of AuNPs (b). When CTAB was added to the Ars-3 aptamer solution, most of the CTAB would be exhausted due to the formation of supramolecules with DNAs. In this case, the following AuNPs would aggregate slightly (c). Subsequently, increasing concentrations of As(III) were added into the above sensing solutions, and the results show that AuNPs are gradually aggregated (d–f).

Moreover, the average size of the AuNPs was determined by PCS (Table 2), and the results demonstrated that the average size of the AuNPs increased gradually in the presence of increasing concentrations of As(III), which is in accordance with that of TEM observation. These results further supported the supposed principle of the present biosensor for As(III) detection.

3.3. Effect of CTAB on arsenic(III) detection

Based on the above results, the concentration of 1.6 μM was sufficient for CTAB to aggregate the AuNPs. Considering the presence of aptamer and As(III), this concentration may be not suitable for the present biosensor. According to previous experience, 7.5 nM of Ars-3 aptamer was used to interact with 100 and 1000 ppb of As(III), then the varying concentrations of CTAB from 0.8 to 1.6 μM were added into the above solutions. After the addition of AuNPs, the RS intensity and A_{650}/A_{520} were recorded. As shown in Fig. S1 (ESI†), about 1.1 μM of CTAB was the optimal concentration for the present biosensor, where the maximum signal was achieved both at lower and higher concentrations of As(III).

3.4. Effect of aptamer on arsenic(III) detection

The aptamer would play two major roles in the present biosensor: (a) it interacted with As(III) to form an aptamer–As(III) complex; and (b) it assembled supramolecules by CTAB to prevent AuNPs from aggregating. The signals of the present

Table 4 Determination of As(III) in water samples

	Colorimetric assay			RS assay		
Water samples	Mean found/ppb	Recovery (%)	RSD (%)	Mean found/ppb	Recovery (%)	RSD (%)
$As^{(III)}(10)$,[a] $As^{(V)}(5)$, $Ag^{(I)}(20)$, $Cd^{(II)}(10)$, $Mn^{(II)}(15)$, $NO_3^-(40)$, $SO_4^{2-}(15)$	12.4	124	6.5	9.8	98	2.0
$As^{(III)}(20)$, $Pb^{(II)}(20)$, $Ni^{(II)}(10)$, $Ca^{(II)}(30)$, $NO_3^-(40)$, $SO_4^{2-}(10)$, $Cl^-(60)$	22.5	113	7.1	21.4	107	2.3
$As^{(III)}(50)$, $Pb^{(II)}(40)$, $Cu^{(II)}(60)$, $Zn^{(II)}(50)$, $Ca^{(II)}(80)$, $NO_3^-(80)$, $SO_4^{2-}(60)$, $Cl^-(260)$	47.3	94.6	5.3	58.5	117	4.5
$As^{(III)}(80)$, $As^{(V)}(60)$, $Pb^{(II)}(100)$, $Ni^{(II)}(80)$, $NO_3^-(200)$, $SO_4^{2-}(80)$	82.2	103	5.5	76.6	95.8	2.7
$As^{(III)}(100)$, $Mg^{(II)}(100)$, $Ni^{(II)}(80)$, $Zn^{(II)}(120)$, $Fe^{(II)}(60)$, $SO_4^{2-}(240)$, $Cl^-(240)$	97.7	97.7	6.4	102	102	3.3
$As^{(III)}(500)$, $Cd^{(II)}(600)$, $Ca^{(II)}(400)$, $Fe^{(II)}(200)$, $NO_3^-(1200)$, $SO_4^{2-}(200)$, $Cl^-(800)$	523	105	6.1	473	94.6	4.7
$As^{(III)}(1000)$, $Pb^{(II)}(800)$, $Ni^{(II)}(1000)$, $NO_3^-(1600)$, $SO_4^{2-}(1000)$	1060	106	8.2	975	97.5	5.4

[a] Final concentration (ppb) of ions was added.

biosensor depended on the aggregation of the AuNPs, and thus the concentration of the aptamer may be critical to the efficiency of the biosensor for As(III) detection. To obtain the optimal sensing conditions, the varying concentrations of Ars-3 aptamer in the range of 1–50 nM were used. As can be observed in Fig. S2 (ESI†), the maximum signals were achieved at 10 and 15 nM of Ars-3 aptamer under lower (100 ppb) and higher (1000 ppb) concentrations of As(III), respectively. To maintain the high sensitivity of the biosensor under lower concentrations of target, about 10 nM of Ars-3 aptamer was used in subsequent experiments.

3.5. Sensitivity of the biosensor for arsenic(III) detection

To evaluate the sensitivity of the present biosensor, different concentrations of As(III) from 1 to 1500 ppb were added into the sensing solutions, and the signals of RS intensity and absorbance values at 520 nm and 650 nm were recorded. As shown in Fig. 5(a), AuNPs aggregated gradually with increasing concentrations of As(III), and the color of the sensing solutions changed gradually from wine red, purple, blue, to grey. When the concentration of As(III) was over 40 ppb, the color of the sensing solution could be distinguished by the naked eye from that of the blank sample.

To quantify the detection limit of the present biosensor, the variations of RS intensity (ΔI) and absorbance values (ΔA) at 520 nm and 650 nm were plotted, and the calibration curves (Fig. 5b and c) looked like the sigmoid shapes, which were fitted to a Hill plot with the correlation coefficient of 0.997 and 0.998. It can be observed that the absorbance and RS intensity had changed slightly when the concentrations of As(III) were over 400 ppb in the sensing solutions, which indicated that the binding interaction between the aptamer and As(III) had reached a balance and saturation. Thus the saturated binding ratio of As(III) to aptamer is calculated as about 550 : 1 (molar ratio) in the present biosensor. The ΔA at low As(III) concentrations was fitted to a linear expression with the equation of $y = 3.54 \times 10^{-3}x + 0.012$ ($R = 0.996$), where ΔI was fitted to the equation of $y = 0.022x + 0.013$ ($R = 0.994$). Based on our previous reports,[35,43] 3σ/slope was used to determine the detection limit of the biosensor, as low as 0.6 ppb for the colorimetric assay and 0.77 ppb for the RS assay, which are lower than the US EPA and WHO defined toxicity levels of arsenic in drinking water (10 ppb). The present biosensor is more sensitive than our previous report,[35] where a cationic polymer was used to aggregate the AuNPs. This difference in the sensitivity may be ascribed to the fierce aggregation of AuNPs caused by cationic polymers, which would result in a high background signal in the detection of As(III).

AuNPs were used as an ideal material for signal output, so their properties may affect the sensitivity of the present biosensor. Herein, a variety of AuNPs with different sizes in the range of 18–80 nm were employed to detect As(III), and the results were summarized in Table 3. The data show that the assay sensitivity is associated with the particle diameter. As the particle diameter increases, the detection limit deteriorates gradually and its value has increased by one order of magnitude when the particle size is 80 nm. This phenomenon may be attributed to a relatively higher background signal and lower aggregation efficiency of large-diameter AuNPs. Moreover, suitable amounts of some other cationic surfactants and salt were also used for sensitivity studies. As shown in Table 3, the detection limits of the cationic surfactants-mediated biosensor are lower than that of the salt-induced biosensor. The results indicate that cationic surfactants indeed possess potential application in the sensitive detection of targets by the AuNPs-based sensors.

3.6. Selectivity of the biosensor for arsenic(III) detection

The selectivity of the biosensor for As(III) detection was also investigated. A variety of competing metal ions, including As(V), Pb(II), Cd(II), Hg(II), Ag(I), Mg(II), Zn(II), Mn(II), Ni(II), Cu(II), Fe(II) and Ca(II), were individually added to the sensing solutions, and the variations of absorbance values (ΔA) were calculated. Fig. 6 shows the difference in the color and ΔA between blank and solutions containing 100 and 1000 ppb of As(III) and other metal ions. The results demonstrate that all of the metal ions display slight and negligible interferences on the biosensor for As(III) detection.

3.7. Velocity of the biosensor for arsenic(III) detection

The speed of signal output is an important parameter of a biosensor for sensing the target. In some cases, a rapid assay is needed to meet the demand of on-site and real-time arsenic detection. To evaluate the velocity of the present biosensor, the kinetics of absorbance variations in the presence of various concentrations of As(III) were investigated. As shown in Fig. S3 (ESI†), the signals attained their top values in less than 2 min both at higher and lower target concentrations. These results clearly indicate that the speed of the present biosensor for As(III) detection is rapid.

3.8. Detection of arsenic(III) in water samples

The applications of the present biosensor based on colorimetric and RS assays were evaluated for the determination of As(III) in several water samples containing different concentrations of As(III) and some other metal cations and anions. The results are summarized in Table 4, which displays that the mean recovery of samples was in the range of 94.6–124% and the relative standard deviation (RSD) was between 2.0 and 8.2%. The results reveal the potential application of the present biosensor for As(III) detection in water samples.

4. Conclusions

In conclusion, we have successfully developed an aptamer biosensor with high sensitivity and specificity for As(III) detection through colorimetric and RS assays. The principle of such a biosensor is based on the aggregation of AuNPs that is controlled by the special interactions among the arsenic-binding aptamer, CTAB and As(III). In the presence of As(III), the aptamer is exhausted firstly to the formation of an aptamer–As(III) complex, so that the subsequent CTAB addition aggregates the AuNPs, which leads to remarkable variations of absorbance and RS intensity. The detection limit of our approach is about 40 ppb for the naked eye and 0.6 ppb for machine assays, with a high selectivity over other competitive

metal ions. In addition, the present biosensor is rapid and reliable for As(III) detection in water samples. The experimental results reported here will offer the possibility of a rapid, reliable, highly sensitive and selective monitoring method for As(III) from environmental samples.

Acknowledgements

This work was supported by the National High-Tech Research and Development Plan (2012AA101405), the Special Fund for Agro-scientific Research in the Public Interest of China (200903056), the National Natural Science Foundation of China (31071860), and the Innovation Fund of Shanghai Jiao Tong University for Postgraduate.

References

1 K. H. Morales, L. Ryan, T. L. Kuo, M. M. Wu and C. J. Chen, *Environ. Health Perspect.*, 2000, **108**, 655–661.
2 M. A. Ferreira and A. A. Barros, *Anal. Chim. Acta*, 2002, **459**, 151–159.
3 M. Argos, T. Kalra, P. J. Rathouz, Y. Chen, B. Pierce, F. Parvez, T. Islam, A. Ahmed, M. Rakibuz-Zaman, R. Hasan, G. Sarwar, V. Slavkovich, A. van Geen, J. Graziano and H. Ahsan, *Lancet*, 2010, **376**, 252–258.
4 A. A. Ensafi, A. C. Ring and I. Fritsch, *Electroanalysis*, 2010, **22**, 1175–1185.
5 K. A. Francesconi and D. Kuehnelt, *Analyst*, 2004, **129**, 373–395.
6 D. E. Mays and A. Hussam, *Anal. Chim. Acta*, 2009, **646**, 6–16.
7 V. C. Ezeh and T. C. Harrop, *Inorg. Chem.*, 2012, **51**, 1213–1215.
8 M. Berg, P. T. K. Trang, P. H. Viet, N. Van Mui and J. R. Van Der Meer, *Environ. Sci. Technol.*, 2005, **39**, 7625–7630.
9 J. R. Kalluri, T. Arbneshi, S. A. Khan, A. Neely, P. Candice, B. Varisli, M. Washington, S. McAfee, B. Robinson, S. Banerjee, A. K. Singh, D. Senapati and P. C. Ray, *Angew. Chem., Int. Ed.*, 2009, **48**, 9668–9671.
10 K. de Mora, N. Joshi, B. L. Balint, F. B. Ward, A. Elfick and C. E. French, *Anal. Bioanal. Chem.*, 2011, **400**, 1031–1039.
11 J. W. Liu, Z. H. Cao and Y. Lu, *Chem. Rev.*, 2009, **109**, 1948–1998.
12 I. Willner, B. Shlyahovsky, M. Zayats and B. Willner, *Chem. Soc. Rev.*, 2008, **37**, 1153–1165.
13 S. P. Song, L. H. Wang, J. Li, J. L. Zhao and C. H. Fan, *TrAC, Trends Anal. Chem.*, 2008, **27**, 108–117.
14 K. Sefah, J. A. Phillips, X. L. Xiong, L. Meng, D. Van Simaeys, H. Chen, J. Martin and W. H. Tan, *Analyst*, 2009, **134**, 1765–1775.
15 M. Famulok, J. S. Hartig and G. Mayer, *Chem. Rev.*, 2007, **107**, 3715–3743.
16 M. X. You, Y. Chen, L. Peng, D. Han, B. C. Yin, B. C. Ye and W. H. Tan, *Chem. Sci.*, 2011, **2**, 1003–1010.
17 J. Liu and Y. Lu, *Angew. Chem., Int. Ed.*, 2007, **46**, 7587–7590.
18 J. W. Liu and Y. Lu, *J. Am. Chem. Soc.*, 2003, **125**, 6642–6643.
19 J. W. Liu, A. K. Brown, X. L. Meng, D. M. Cropek, J. D. Istok, D. B. Watson and Y. Lu, *Proc. Natl. Acad. Sci. U. S. A.*, 2007, **104**, 2056–2061.
20 M. Kim, H. J. Um, S. Bang, S. H. Lee, S. J. Oh, J. H. Han, K. W. Kim, J. Min and Y. H. Kim, *Environ. Sci. Technol.*, 2009, **43**, 9335–9340.
21 B. C. Yin, P. Zuo, H. Huo, X. Zhong and B. C. Ye, *Anal. Biochem.*, 2010, **401**, 47–52.
22 E. Boisselier and D. Astruc, *Chem. Soc. Rev.*, 2009, **38**, 1759–1782.
23 R. Wilson, *Chem. Soc. Rev.*, 2008, **37**, 2028–2045.
24 W. J. Parak, R. A. Sperling, P. Rivera Gil, F. Zhang and M. Zanella, *Chem. Soc. Rev.*, 2008, **37**, 1896–1908.
25 B. C. Ye and B. C. Yin, *Angew. Chem., Int. Ed.*, 2008, **47**, 8386–8389.
26 Z. D. Wang, J. H. Lee and Y. Lu, *Adv. Mater.*, 2008, **20**, 3263.
27 A. Liang, H. Ouyang and Z. Jiang, *Analyst*, 2011, **136**, 4514–4519.
28 M. Zhang and B. C. Ye, *Anal. Chem.*, 2011, **83**, 1504–1509.
29 M. Zhang, Y. Q. Liu and B. C. Ye, *Analyst*, 2012, **137**, 601–607.
30 M. Zhang, Y. Q. Liu and B. C. Ye, *Analyst*, 2011, **136**, 4558–4562.
31 Y. W. Lin, C. C. Huang and H. T. Chang, *Analyst*, 2011, **136**, 863–871.
32 Z. Wang, D. B. Liu and X. Y. Jiang, *Nanoscale*, 2011, **3**, 1421–1433.
33 F. Xia, X. L. Zuo, R. Q. Yang, Y. Xiao, D. Kang, A. Vallee-Belisle, X. Gong, J. D. Yuen, B. B. Y. Hsu, A. J. Heeger and K. W. Plaxco, *Proc. Natl. Acad. Sci. U. S. A.*, 2010, **107**, 10837–10841.
34 Y. Ofir, B. Samanta and V. M. Rotello, *Chem. Soc. Rev.*, 2008, **37**, 1814–1823.
35 Y. Wu, S. Zhan, F. Wang, L. He, W. Zhi and P. Zhou, *Chem. Commun.*, 2012, **48**, 4459–4461.
36 H. Li, Y. Yang, Y. Wang, W. Li, L. Bi and L. Wu, *Chem. Commun.*, 2010, **46**, 3750–3752.
37 M. Schulz-Dobrick, K. V. Sarathy and M. Jansen, *J. Am. Chem. Soc.*, 2005, **127**, 12816–12817.
38 R. Fenger, E. Fertitta, H. Kirmse, A. F. Thünemann and K. Rademann, *Phys. Chem. Chem. Phys.*, 2012, **14**, 9343–9349.
39 X. Cheng, T. Bing, X. Liu and D. Shangguan, *Anal. Chim. Acta*, 2009, **633**, 97–102.
40 X. Liu and N. L. Abbott, *J. Phys. Chem. B*, 2010, **114**, 15554–15564.
41 D. Santhiya, R. S. Dias, A. Shome, P. K. Das, M. G. Miguel, B. Lindman and S. Maiti, *Langmuir*, 2009, **25**, 13770–13775.
42 S. Zhou, D. Liang, C. Burger, F. Yeh and B. Chu, *Biomacromolecules*, 2004, **5**, 1256–1261.
43 Y. Wu, S. Zhan, L. Xu, W. Shi, T. Xi, X. Zhan and P. Zhou, *Chem. Commun.*, 2011, **47**, 6027–6029.
44 G. K. Darbha, A. K. Singh, U. S. Rai, E. Yu, H. Yu and P. Chandra Ray, *J. Am. Chem. Soc.*, 2008, **130**, 8038–8043.
45 P. C. Ray, *Angew. Chem., Int. Ed.*, 2006, **45**, 1151–1154.
46 C. K. Kim, R. R. Kalluru, J. P. Singh, A. Fortner, J. Griffin, G. K. Darbha and P. C. Ray, *Nanotechnology*, 2006, **17**, 3085.

